Islamic Azad University

Journal of Optoelectronical Nanostructures

Journal homepage: https://sanad.iau.ir/journal/jopn

Research Paper

A Comparative Finite Element Analysis of an Atmospheric Pressure Corona Discharge Plasma in Argon Gas

Elnaz Poorreza

[1] Ph. D, Faculty of Electrical engineering, University of Bonab, Bonab, Iran

Article History:

Received: 26.07.2025
Revised: 30.09.2025
Accepted: 01.10.2025
Published: 31.12.2025

Use your device to scan and read the article online

Abstract:

A negative corona discharge is a type of electrical discharge that occurs when a high negative voltage is applied to a sharp or curved electrode relative to a grounded electrode, ionizing the surrounding gas and creating a weakly conductive plasma region. Corona discharge, as a form of non-thermal plasma, has several important applications in nanotechnology, including: surface modification of nano materials, nano coatings and nanoparticle synthesis. In this study, the phenomenon of a negative corona discharge that takes place in the spatial region situated between two conductors has been simulated based on finite element analysis, in comparative manner. The input voltage that is applied varies between 1000 [V], 1500 [V], and 2000 [V]. It has been engineered to be coaxial in their arrangement. In this simulated setup, a negative electric potential is deliberately applied to the inner conductor, while the outer conductor is systematically grounded to provide a reference point for the electric potential. The discharge that is being modeled and subsequently simulated occurs within an environment of argon gas maintained at atmospheric pressure, thereby creating a realistic scenario for the study of such discharge phenomena. Profiles of electron density, electron potential, electron temperature, electron current density, secondary emission flux, were presented in this study.

Keywords:
Argon gas,
Plasma chemistry,
Corona discharge,
Electric potential,
Nano structure

Citation: E. Poorreza, A comparative finite element analysis of an atmospheric pressure corona discharge plasma in argon gas. **Journal of Optoelectronical Nanostructures.** 2025; 10 (4): 1-17.

***Corresponding author: E. Poorreza**
Address: Faculty of Electrical engineering, University of Bonab, Bonab, Iran
Email: e_poorreza@sut.ac.ir, elnaz.prza@gmail.com
DOI: https://doi.org/10.71577/jopn.2025.1213073

1. INTRODUCTION

Plasmas are characterized by a vast array of attributes that encompass thermal energy, ionization fractions, and particle density, and the degree to which these factors manifest, in conjunction with the various assumptions employed in the theoretical frameworks that seek to represent them, plays a significant role in the classification of plasmas into a diverse array of categories. Among the numerous classifications that have been identified are those such as cold plasma [1-4], thermal plasma [5, 6], microwave-assisted plasmas [7-10], and several others, as documented in the literature [11-17]. The phenomenon of corona discharges occurring within air and other gaseous mediums under varying pressure conditions continues to capture the interest and scholarly attention of researchers in the field. Specifically, corona discharge (CD) refers to the breakdown of air that takes place on the surface of a pointed electrode when the local electric field strength at that tip surpasses the established threshold for air breakdown, as explored in previous studies [18, 19].

The occurrence of corona discharge is particularly prominent in proximity to electrodes that possess a high degree of tip curvature, where the electric field intensity attains a level sufficient to instigate the electrical breakdown of gaseous dielectrics. The phenomenon of air micro-gap discharge, which transpires via mechanisms such as electronic excitation, ionization, charge migration, and diffusion, results in the generation of a substantial quantity of freely moving electrons and ions, thereby effectively producing a state of plasma, as detailed in various scholarly works [20].

In the present investigation, the phenomenon characterized by a negative corona discharge, which manifests itself within the spatial region that is strategically positioned between two conductive materials, has been subjected to a simulation that adopts a comparative approach for its thorough analysis. The voltage levels that have been systematically applied during this investigation exhibit a variation, specifically ranging from 1000 volts to 1500 volts and ultimately culminating at 2000 volts, with the resultant data encompassing vital parameters such as electron densities, ion densities, temperatures, and other relevant metrics being meticulously presented for further examination. It is noteworthy that the configuration of the conductors has been engineered to adopt a coaxial arrangement, which is essential for the accurate representation of the discharge phenomena under investigation. Within the confines of this simulated setup, a negative electric potential is purposefully imposed upon the inner conductor, while the outer conductor is methodically grounded to establish a reliable

reference point for the measurement of the electric potential across the system. The discharge that is the focus of this modeling and subsequent simulation occurs within a controlled environment filled with argon gas, which is maintained at atmospheric pressure, thereby facilitating the creation of a realistic and scientifically valid scenario for an in-depth study of such discharge phenomena.

2. MODEL DEFINITION

Figure 1 depicts a cross section of the simulated model. By considering a long and uniform coaxial conductor shape, the model can be viewed as axisymmetric and therefore simplified to a 1D problem.

The model delineated in the subsequent section is employed to replicate the ionization process of the neutral gas (Ar) along with the flux of charged particles (Ar+ and electrons) when a negative electric potential is applied to the inner conductor (cathode). The elevated electric field, engendered by the interplay of high potential and the reduced curvature radius of the conductor (inner conductor, ri), incites electron drift and the ionization of the neutral gas encircling the cathode. The resultant ions facilitate the production of additional electrons via secondary emission at the surface of the cathode. These liberated electrons are propelled through a confined spatial region away from the cathode, allowing them to gain substantial energy. This phenomenon may result in ionization, thereby generating new electron-ion pairs. The secondary ions traverse towards the cathode, where they contribute to the ejection of further secondary electrons. This sequence of events is integral to the maintenance of the discharge. The model is fundamentally grounded in the fluid equations governing electrons and ions, in conjunction with Poisson's equation. Secondary electrons produced by the ion bombardment of the cathode surface are duly considered. The model incorporates a Scharfetter-Gummel upwind scheme to mitigate numerical instabilities in the charged particles' number density that are associated with the finite element method. This is particularly essential in regions proximal to the cathode, where the ion flux is markedly elevated.

This particular study meticulously simulates the phenomenon of a negative corona discharge that takes place in the spatial region situated between two conductors that have been meticulously engineered to be coaxial in their arrangement. In this simulated setup, a negative electric potential is deliberately applied to the inner conductor, while the outer conductor is systematically grounded to provide a reference point for the electric potential. The discharge that is being modeled and subsequently simulated occurs within an environment of argon gas maintained at atmospheric pressure, thereby creating a realistic scenario for the study of such discharge phenomena.

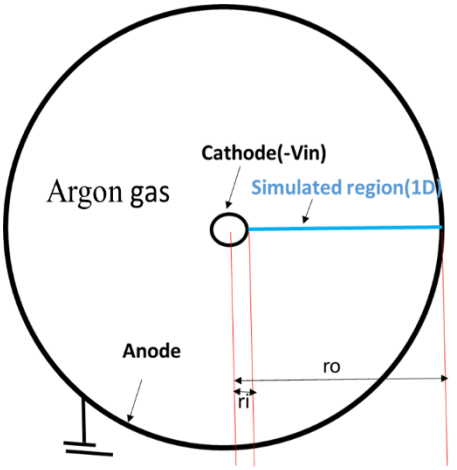

Fig. 1. Configuration of coaxial cross section. The negative potential (-Vin) is exerted at the inner conductor (cathode) and the outer electrode is grounded (anode).

3. DOMAIN EQUATIONS

The calculation of electron density is achieved by solving the drift-diffusion equation pertaining to the electron density [21, 22].

$$\frac{\partial}{\partial t}(n_e) + \boldsymbol{\nabla} \cdot [-n_e[(\mu_e \cdot \boldsymbol{E}) - D_e \cdot \boldsymbol{\nabla} n_e] = R_e \qquad (1)$$

$$\frac{\partial}{\partial t}(n_\varepsilon) + \boldsymbol{\nabla} \cdot [-(n_\varepsilon(\mu_\varepsilon \cdot \boldsymbol{E}) - D_\varepsilon \boldsymbol{\nabla} n_\varepsilon] + \boldsymbol{E} \cdot \Gamma_e = R_\varepsilon \qquad (2)$$

The electron source, denoted as Re, alongside the energy dissipation resulting from inelastic collisions, represented as Rε, will be elucidated in subsequent sections. The parameters of electron diffusivity, energy mobility, and energy diffusivity are derived from the electron mobility through established mathematical relationships.

$$D_e = \mu_e T_e \qquad (3)$$

$$\mu_\varepsilon = 5/3\mu_e \qquad (4)$$

$$D_\varepsilon = \mu_\varepsilon T_e \qquad (5)$$

The coefficients pertaining to the source in the aforementioned equations are ascertained through the analysis of plasma chemistry employing rate coefficients. Let us assume the existence of *M* reactions that play a role in the augmentation or reduction of electron density, alongside *P* inelastic electron-neutral collision

occurrences. Generally speaking, with regard to rate coefficients, the source term associated with electrons is articulated as follows.

$$R_e = \sum_{j=1}^{M} x_j \, k_j N_n n_e \qquad (6)$$

where x_j represents the mole fraction of the specific species pertinent to reaction j, k_j denotes the rate coefficient associated with reaction j (SI unit: m^3/s), and N_n signifies the overall neutral number density (SI unit: $1/m^3$). The energy loss experienced by electrons is derived by aggregating the collisional energy losses across all relevant reactions:

$$R_\varepsilon = \sum_{j=1}^{P} x_j \, k_j N_n n_e \Delta\varepsilon_j \qquad (7)$$

Here, $\Delta\varepsilon_j$ represents the energy dissipation associated with reaction j (SI unit: V). The rate coefficients may be derived from cross-section data through the integration of the following expressions:

$$k_k = \gamma \int_0^\infty \varepsilon \, \sigma_k(\varepsilon) f(\varepsilon) d\varepsilon \qquad (8)$$

where γ = (2q/me) 1/2 (SI unit: C1/2/kg1/2), with me denoting the mass of the electron (SI unit: kg), ε indicating the energy (SI unit: V), σk representing the collision cross section (SI unit: m2), and f signifying the electron energy distribution function. In this context, a Maxwellian electron energy distribution function (EEDF) is presumed. For species other than electrons, the subsequent equation is employed to ascertain the mass fraction of each respective species:

$$\frac{\partial}{\partial t}(w_k) + \rho(u \cdot \boldsymbol{\nabla}) w_k = R_k + \boldsymbol{\nabla} \cdot j_k \qquad (9)$$

The computation of the electrostatic field is executed utilizing the equation:

$$-\boldsymbol{\nabla} \cdot \varepsilon_0 \varepsilon_r \boldsymbol{\nabla V} = \boldsymbol{\rho} \qquad (10)$$

The space charge density ρ is derived automatically in accordance with the plasma chemistry delineated in the model, employing the formula.

$$\rho = \sum_{K=1}^{N} z_K \, n_k - n_e \qquad (11)$$

3.1. BOUNDARY CONDITIONS

Electrons are relinquished to the wall as a consequence of stochastic motion occurring within a few mean free paths of the boundary, while simultaneously being acquired through secondary emission phenomena, thereby producing the boundary condition for the flux of electron energy.

$$\mathrm{n} \cdot \Gamma_e = (1/2) V_{e.th} n_e - \sum_P \gamma_P \, (\Gamma_P . \mathrm{n}) \quad (12)$$

For the electron flux:

$$\mathrm{n} \cdot \Gamma_\varepsilon = (5/6) V_{e.th} n_\varepsilon - \sum_P \varepsilon_P \gamma_P (\Gamma_P . \mathrm{n}) \quad (13)$$

The second term on the right-hand side of Equation 1 denotes the acquisition of electrons attributed to secondary emission processes, where γ_p represents the secondary emission coefficient. The second term in Equation 2 signifies the flux of energy associated with secondary emissions, with ε_p denoting the average energy of the secondary electrons. In the case of heavier species, ions are expelled to the wall as a result of surface interactions and the orientation of the electric field towards the boundary:

$$n \cdot J_k = \quad M_w \, R_K + \quad M_w \, c_K \, \mathrm{Z} \, \mu_K \, (\mathrm{E} \cdot \mathrm{n}) \, [\quad Z_K \, \mu_K (\mathrm{E} \cdot \mathrm{n}) > 0] \quad (14)$$

The discharge phenomenon is induced by a direct current electric potential (V0) that is applied to the inner conductor within the coaxial configuration (at the radial coordinate $r = r_i$). The opposing boundary (at the radial coordinate $r = r_o$) is maintained at ground potential. In order to initiate the numerical simulation, a step function is employed to modulate V_0 with the transiently applied potential, which adopts the following mathematical representation.

$$V = V_0 \tanh(t/\tau) \quad (15)$$

where the mathematical function $\tanh(t/\tau)$ is employed to produce the voltage step function (−1000 V). The alternative boundary (located at the coordinate $r = r_o$) is maintained at ground potential.

It is important to note that, by the simulation, the cathode is subjected to a substantial flux of ions that results in a significant generation of secondary electrons which, in turn, exacerbates the bombardment of the cathode by ions and

perpetuates the cycle. To mitigate the potential for this avalanche effect to escalate without limit, a resistor-capacitor (RC) circuit has been incorporated in series with the overall system. To accurately represent the inclusion of this circuit, the voltage at the inner conductor is adjusted utilizing the differential equation.

$$V = V_0 - I_p R_b + R_b C_b \frac{\partial V}{\partial t} \qquad (16)$$

where I_p is defined as:

$$I_P = -\int (n \cdot J_I + n \cdot J_e + \frac{\partial}{\partial t}(n \cdot D))dS \qquad (17)$$

and where $n \cdot J_i$ is the normal component of the total ion current density at the wall, $n \cdot J_e$ is the normal component of the total electron current density at the wall, and $n \cdot D$ the normal electrical displacement at the surface

3.2. PLASMA CHEMISTRY

Argon presents itself as a compelling gas for utilization in benchmark problems due to the limited number of reactions and species that necessitate consideration. Table 1 enumerates the chemical reactions that have been taken into account.

Table 1. Table of reactions

Reaction	Formula	Type	Δε(ev)
1	e + Ar => e + Ar	Elastic	0
2	e + Ar => e + Ars	Excitation	11.5
3	e + Ars => e + Ar	Super-elastic	-11.5
4	e + Ar => 2e + Ar^+	Ionization	15.8
5	e + Ars => 2e + Ar^+	Ionization	4.24
6	Ars + Ars => e + Ar + Ar^+	Penning ionization	-
7	Ars + Ar => Ar + Ar	Metastable quenching	-

At the outset, a minimal quantity of seed electrons exists. These electrons are imperative for the initiation of the discharge process. In conjunction with the

volumetric reactions, the subsequent surface reactions are incorporated in Table 2:

Table 2. Table of surface reactions

Reaction	Formula	Sticking coefficient
1	Ars => Ar	1
2	Ar+ => Ar	1

Upon reaching the wall, the ionized atoms are posited to revert to neutral argon atoms and transfer their charge to the wall. It is noteworthy that the secondary emission coefficient is designated as 0.2 at the cathode boundary (located at coordinate $r = r_i$) and as 0 at the outer electrode (located at coordinate $r = r_o$). The average energy of the secondary electrons is established at 4 eV.

4. Results And Discussion

Analyzing the temporal progression of the densities during the computational procedure reveals that the gas is initially characterized by a low degree of ionization (with electrons and ions exhibiting comparatively diminished densities relative to neutral atoms). Utilization of a negative voltage to the cathode, the highly mobile electrons experience acceleration towards the anode, that results in the formation of a positively charged gas in the vicinity of the cathode. With an escalation of the negative potential, the incidence of ion bombardment on the cathode surface intensifies, thereby generating additional secondary electrons, which in turn ionize an increasing number of neutral atoms, culminating in a heightened ion current. As the negative potential escalates, the population of charged particles expands as a direct outcome of this avalanche phenomenon. As the ion current attains greater significance, the RC circuit mitigates the cathode's negative potential, establishing an equilibrium between the generation of charged particles, thus averting the transition of the plasma into an arcing regime. Figure 2 shows the electron and ion densities at the end of the simulation (t = 0.1 s) during which the applied voltage experiences differences across three distinct levels of: (a) 1000 volts, (b) 1500 volts, and (c) 2000 volts. It can be seen that by increasing the voltage, the maximum values of ions and electrons increase. It is noteworthy that the figure employs a log-log scale for its representation. In the figure, one can discern that the ion density is approximately three orders of magnitude greater than the electron density in the proximity of the cathode. The diminutive positive space charge distribution engendered by the ion density delineates an ionization

region that effectively screens the cathode potential from the anode. This phenomenon can be elucidated by presenting the electric potential along the radius of the coaxial assembly; refer to Figure 3.

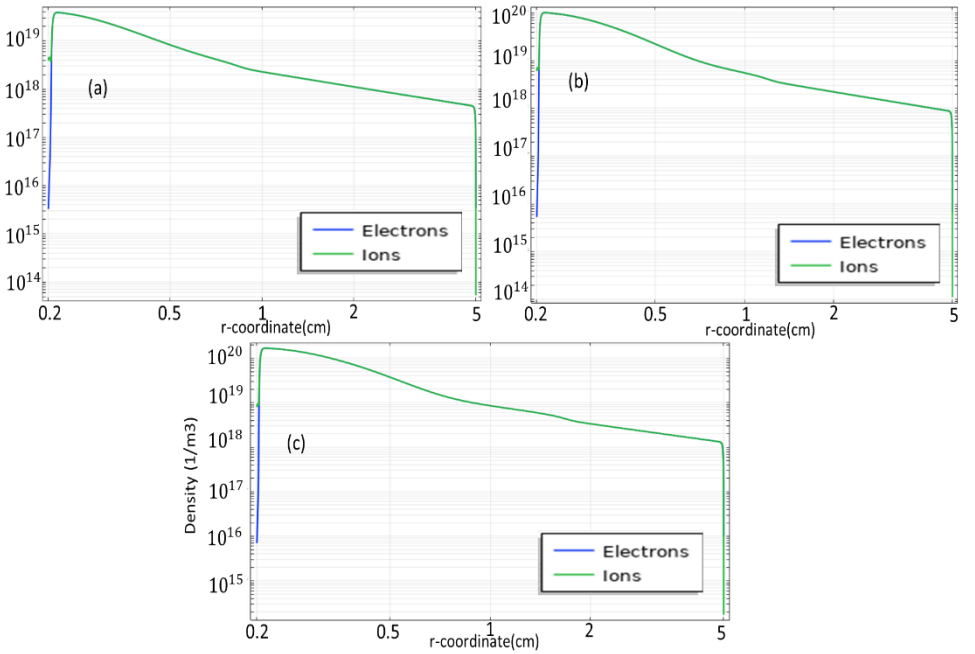

Fig. 2. Plots of electron (blue) and ion (green) number density at the end of the simulation (t = 0.1 s) when the voltage varies between (a) 1000 [V], (b) 1500 [V], (c) and 2000 [V]

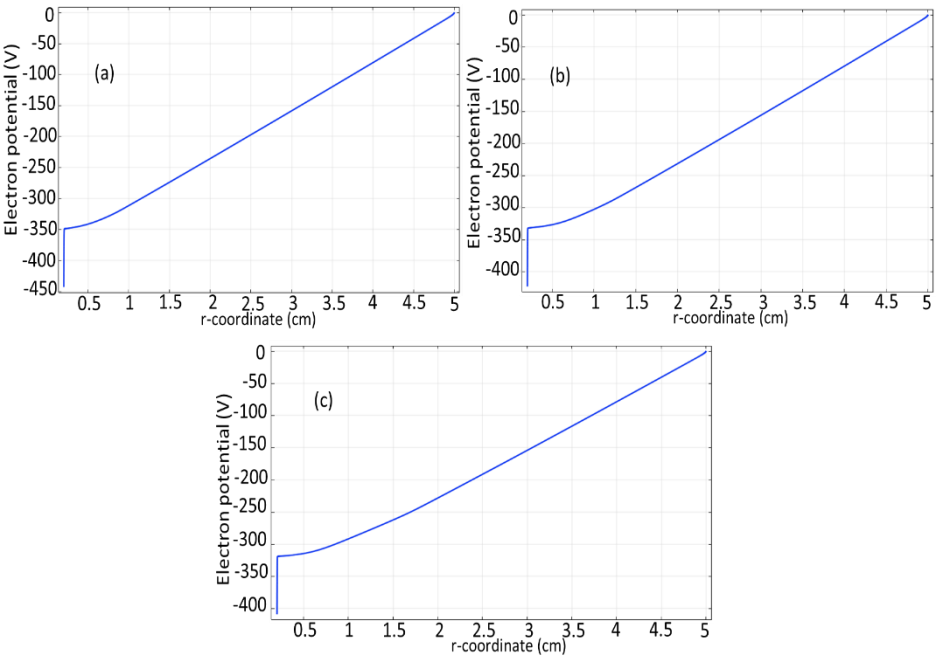

Fig. 3. Electric potential along the radius of the coaxial assembly at the end of the simulation (t = 0.1 s) when the voltage varies between (a) 1000 [V], (b) 1500 [V], (c) and 2000 [V]

The elevated voltage and significant current density present at the cathode contribute to an increase in the electron temperature adjacent to the electrode, thereby facilitating the ionization of neutral atoms within the ionization region. This phenomenon is illustrated in Figure 4, which depicts the electron temperature at the conclusion of the simulation.

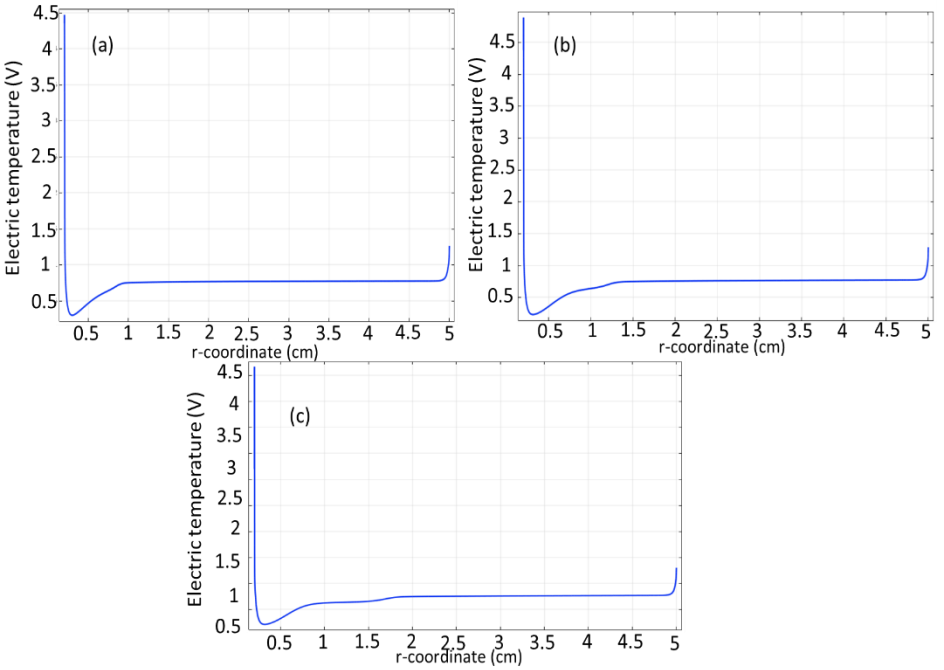

Fig. 4. Electron temperature along the radius of the assembly at the end of the simulation (t = 0.1 s) when the voltage varies between (a) 1000 [V], (b) 1500 [V], (c) and 2000 [V]

In order to investigate the influence of the RC circuit on the system, it is necessary to graph the secondary electron flux as a function of time at the cathode surface as shown in the Figure 5. A thorough examination of the figure indicates a swift increase in the flux, which appears to stabilize as the circuit experiences elevated currents. Additionally, Figure 6 presents the potential at both electrodes as a function of time. A comparative analysis of Figure 5 and Figure 6 elucidates the impact of the circuit on both potential and secondary emission at the cathode surface. Furthermore, a similar effect can be discerned by plotting the electron current density at the electrodes, as shown in Figure 6. This analysis reveals a direct correlation between the secondary emission at the cathode (characterized by positive current flow), the recombination at the anode (indicated by negative flow), and the RC circuit. Finally, Figure 7 illustrates a surface plot of the logarithm of the electron density at the final time step. Figure 8 shows the 2D electron density (log of n_e) at the last time step when the input voltage varies

between (a) 1000 [V], (b) 1500 [V], (c) and 2000 [V]. it can be seen that by elevating the voltage the maximum density of electrons is increased near the electrode.

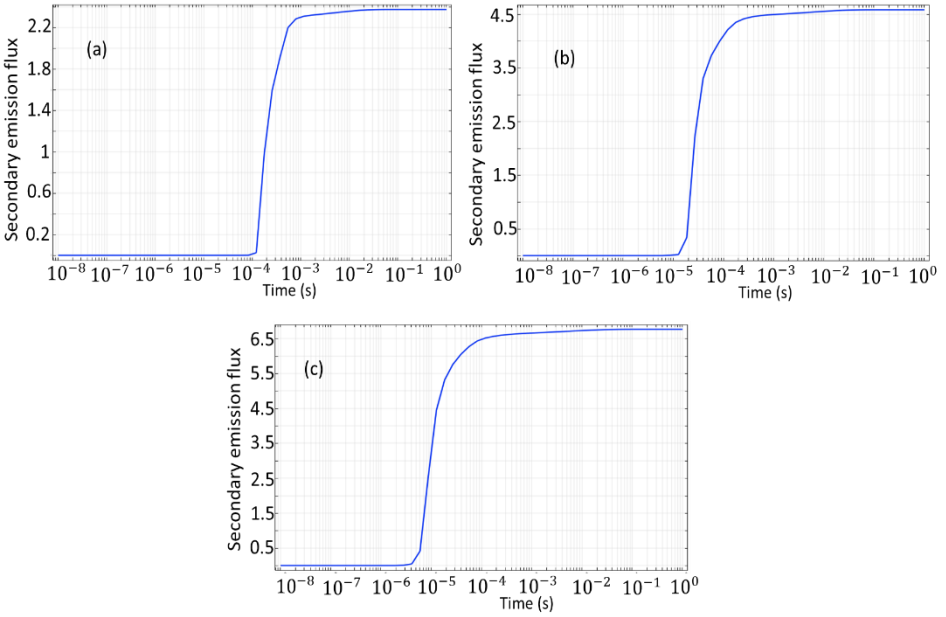

Fig. 5. Secondary emission flux along time at the cathode when the voltage varies between (a) 1000 [V], (b) 1500 [V], (c) and 2000 [V]

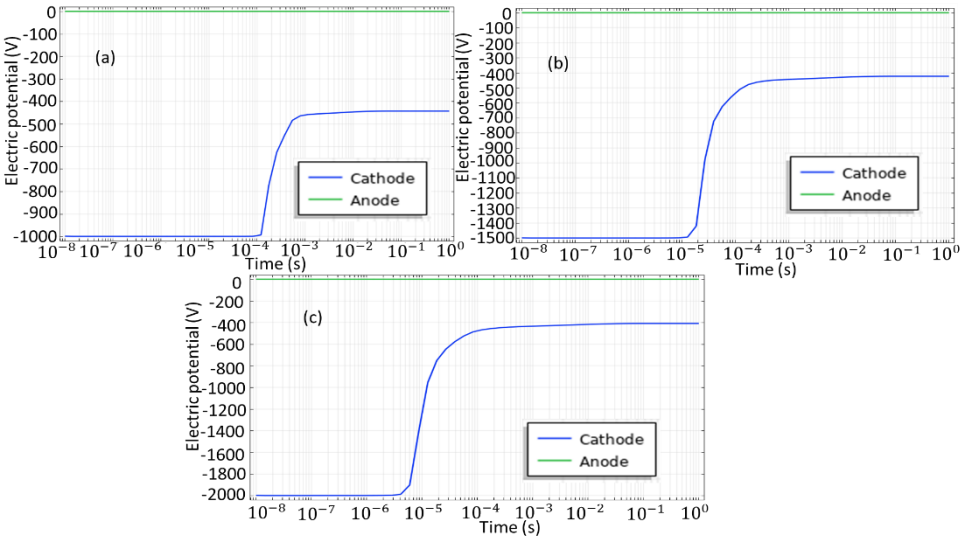

Fig. 6. Potential at the electrodes as a function of time when the voltage varies between (a) 1000 [V], (b) 1500 [V], (c) and 2000 [V]

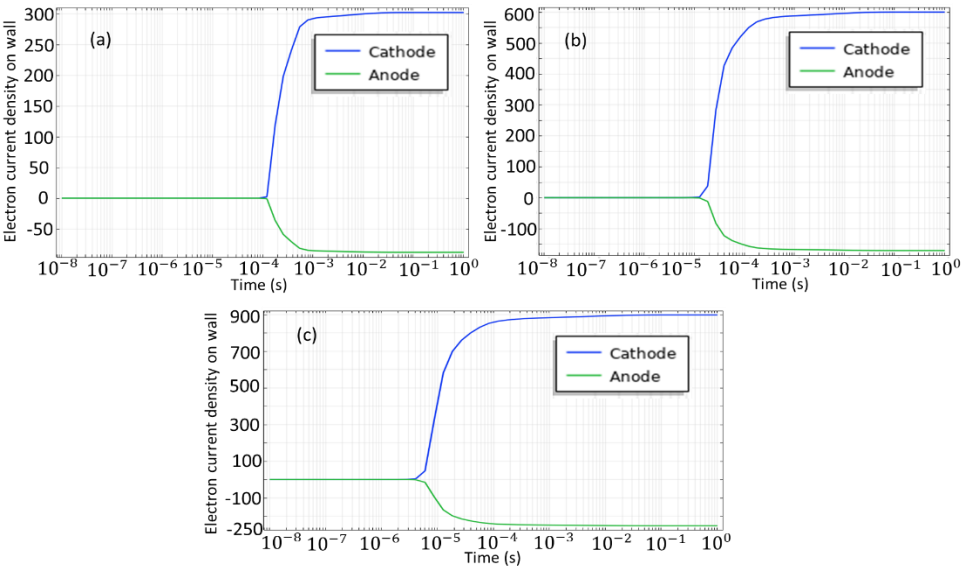

Fig. 7. Electron current density at the electrodes as a function of time when the input voltage varies between (a) 1000 [V], (b) 1500 [V], (c) and 2000 [V]

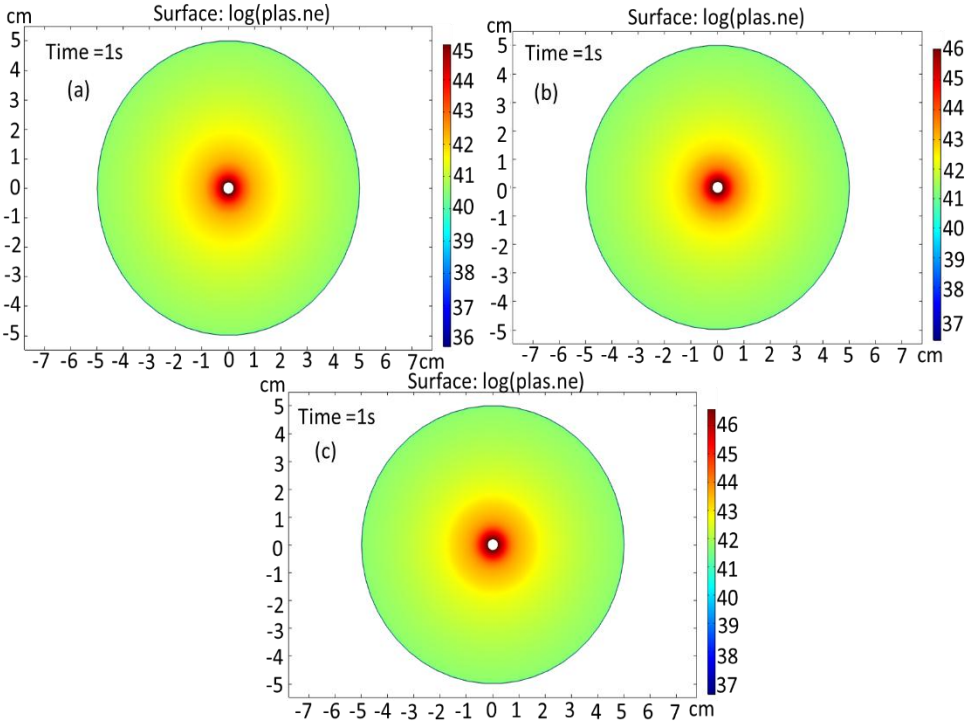

Fig. 8. 2D electron density (log of ne) at the last time step when the voltage varies between (a) 1000 [V], (b) 1500 [V], (c) and 2000 [V]

4. CONCLUSION

In the present investigation, the phenomenon of negative corona discharge occurring in the spatial region situated between two conductive materials has been simulated in a comparative manner. The voltage applied ranges from 1000 [V] to 2000 [V], with corresponding results including electron densities, ion density, temperature, among other parameters being presented. The arrangement has been specifically designed to be coaxial. Within this simulated framework, a negative electric potential is intentionally applied to the inner conductor, while the outer conductor is methodically grounded to establish a reference point for the electric potential. The discharge that is modeled and subsequently simulated transpires within an argon gas environment maintained at atmospheric pressure, thus creating a realistic context for the examination of such discharge phenomena.

REFERENCES

[1] L. Gan *et al.*, Cold atmospheric plasma applications in dermatology: A systematic review, *Journal of Biophotonics*, 14 (3), e202000415, (2021). http://dx.doi.org/10.1002/jbio.202000415

[2] R. R. Khanikar and H. Bailung, Cold Atmospheric Pressure Plasma Technology for Biomedical Application, in *Plasma Science and Technology*: IntechOpen, (2021). http://dx.doi.org/10.5772/intechopen.98895

[3] P. Zheng *et al.*, Spatial distribution characteristics of atmospheric pressure solution cathode glow discharge plasma based on Abel inversion, *Journal of Analytical Atomic Spectrometry*, 40(5), (2025) 1284-1296. http://dx.doi.org/10.1039/D4JA00421C

[4] M. Imran, N. U. Rehman, and N. Wali, Effect of pressure and current density on metastable argon dynamics in low-pressure Ar-O2 plasma, *Physica Scripta*, 100 (2), (2025) 025606. http://dx.doi.org/10.1088/1402-4896/ada315

[5] J. Yang *et al.*, Efficient degradation of Bisphenol A by dielectric barrier discharge non-thermal plasma: Performance, degradation pathways and mechanistic consideration, *Chemosphere*, vol. 286, (2022) 131627. http://dx.doi.org/10.1016/j.chemosphere.2021.131627

[6] S. Elaissi and N. A. Alsaif, Modelling of Nonthermal Dielectric Barrier Discharge Plasma at Atmospheric Pressure and Role of Produced Reactive Species in Surface Polymer Microbial Purification, *Polymers*, 15(5), (2023) 1235. http://dx.doi.org/10.3390/polym15051235

[7] M. Ong, S. Nomanbhay, F. Kusumo, and P. Show, Application of microwave plasma technology to convert carbon dioxide (CO2) into high value products: A review, *Journal of Cleaner Production*, 336, (2022) 130447. http://dx.doi.org/10.1016/j.jclepro.2022.130447

[8] T. Belmonte, T. Gries, R. Cardoso, G. Arnoult, F. Kosior, and G. Henrion, Chemical vapour deposition enhanced by atmospheric microwave plasmas: a large-scale industrial process or the next nanomanufacturing tool?, *Plasma Sources Science and Technology*, 20(2), (2011) 024004. http://dx.doi.org/10.1088/0963-0252/20/2/024004

[9] I. Abramov, E. Gospodchikov, and A. Shalashov, Nonlinear Interaction of Microwave Radiation with a Plasma Flow under Hybrid Resonance Conditions, *Journal of Experimental and Theoretical Physics*,129(3), (2019) 444-454. http://dx.doi.org/10.1134/S106377611907001X

[10] J. F. de la Fuente, A. A. Kiss, M. T. Radoiu, and G. D. Stefanidis, Microwave plasma emerging technologies for chemical processes, *Journal of Chemical Technology & Biotechnology*, vol. 92(10), , (2017) 2495-2505. http://dx.doi.org/10.1002/jctb.5205

[11] I. Piskarev, The role of ozone in chemical processes in electric discharge plasma, *High Energy Chemistry*, 54 (3), (2020) 205-209. http://dx.doi.org/10.1134/S001814392003011X
[12] K. Averin, R. Borisov, and Y. A. Lebedev, Microwave Discharge in Liquid Hydrocarbons: Study of a Liquid Hydrocarbon after Its Discharge Treatment Including Air Bubbling, *High Energy Chemistry*, (54), (2020), 210-216. http://dx.doi.org/10.1134/S0018143918040100
[13] Y. A. Lebedev, A. Tatarinov, and I. Epshtein, Simulation of Microwave Discharge in Liquid n-Heptane in the Presence of Argon in the Discharge Region, *High Energy Chemistry*, 54, (2020) 217-226. http://dx.doi.org/10.1002/ppap.201800198
[14] A. Y. Ryabov, S. Kudryashov, and A. Ochered'ko, "Effect of the Volumetric Flow Rate of Reaction Mixture Components on Nonoxidative Reforming of Methane with Admixed Water in Dielectric-Barrier Discharge," *High Energy Chemistry*, 53, (2019) 478-481.
[15] C. Hertwig, N. Meneses, and A. Mathys, Cold atmospheric pressure plasma and low energy electron beam as alternative nonthermal decontamination technologies for dry food surfaces: A review, *Trends in Food Science & Technology*, 77, (2018) 131-142. http://dx.doi.org/10.1016/j.tifs.2018.05.011
[16] A. Hafeez, F. Javed, T. Fazal, N. Shezad, M. S. ur Rehman, and F. Rehman, Intensification of ozone generation and degradation of azo dye in non-thermal hybrid corona-DBD plasma micro-reactor, *Chemical Engineering and Processing-Process Intensification*, 159, (2021) 108205. http://dx.doi.org/10.1016/j.cep.2020.108205
[17] E. Poorreza and R. H. Vafaie, A Comparative Investigation of an Argon Dielectric Barrier Discharge Reactor under the Variation of Plasma Conditions for Optimization of Power Deposition, *Theoretical Foundations of Chemical Engineering*, 57(6), (2023) 1552-1571. http://dx.doi.org/10.1134/S0040579523330059
[18] X. Guo, L. Zhang, Z. Ji, Y. Gao, Z. Wang, and N. Zhao, Three-Dimensional Simulation of Corona Discharge in a Double-Needle System during a Thunderstorm, *Atmosphere*, 14(5), (2023) 789.
[19] E. Bazelyan, Y. P. Raizer, and N. Aleksandrov, The effect of space charge produced by corona at ground level on lightning attachment to high objects, *Atmospheric Research*, 153, (2015) 74-86. http://dx.doi.org/10.1016/j.atmosres.2014.07.018
[20] Z. Sun, Z. K. Shao, X. Sun, and W. F. Sun, Trichel pulse characteristics and mechanism of negative corona discharge in sub-millimeter gaps, *Physics of Plasmas*, 30(6), (2023). http://dx.doi.org/10.1063/5.0145301

[21] E. Poorreza and N. Dadashzadeh Gargari, Modeling and Simulation of a Microwave-Assisted Plasma with Different Input Power for Plasma-Based Applications, *Russian Journal of Physical Chemistry B,* 17(3), (2023) 719-724, doi: 10.1134/S1990793123030235.
[22] E. Poorreza and N. Dadashzadeh Gargari, Study of the Time Dependence and One Dimentional Simulation of a Dielectric Barrier Discharge Reactor Driven by Sinusoidal High-Frequency Voltage, *Russian Journal of Physical Chemistry B,* 17(3), (2023) 631-645, doi: 10.1134/S1990793123030107.